Journal of The Electrochemical Society, **162** (12) B291-B297 (2015)
0013-4651/2015/162(12)/B291/7/$33.00 © The Electrochemical Society

A Sensitive DNA Biosensor Using Graphene Oxide as the Multi-Site Platform for Probe DNA Immobilization

Feng Gao,[a,b,z] Xili Cai,[a] Hidekazu Tanaka,[b] Qionghua Zhu,[a] Fei Gao,[a] and Qingxiang Wang[a,z]

[a]*Department of Chemistry and Environment Science, Fujian Province University Key Laboratory of Analytical Science, Minnan Normal University, Zhangzhou 363000, People's Republic of China*
[b]*Department of Chemistry, Graduate School of Science and Engineering, Shimane University, Matsue, Shimane 690-8504, Japan*

An ultrasensitive DNA biosensor was constructed in this work by using graphene oxide nanosheets (GONs) as the multi-site platform for probe DNA immobilization. First, *L*-cysteine (*L*-cys) was self-assembled on a gold electrode surface based on the Au-S chemistry. Then the GONs and amino modified probe DNA was covalently grafted to *L*-cys/AuE surface in turn, with the aid of 1-(3-Dimethylanminopropyl)-3-ethylcarbodiimide hydrochloride (EDC) and N-Hydroxy succinimide (NHS). The layer upon layer assembly process was characterized with atomic force microscopy and electrochemical methods. Due to the nano-size effect and multiple site characteristic of GONs, the immobilization density of the probe DNA was determined to be as high as 5.72×10^{-10} mol cm^{-2} using methylene blue as the redox probe. The hybridization experiments showed that the biosensor can quantitatively detect target DNA in a wide range from 1.0×10^{-15} M to 1.0×10^{-9} M with a detection limit of 5.0×10^{-16} M. The selectivity experiments showed that the sensing system could accurately discriminate the complementary sequence from the base mismatched and non-complementary sequences.

Manuscript submitted February 3, 2015; revised manuscript received July 6, 2015. Published August 20, 2015.

With the development of biotechnology, simple, fast and sensitive detection of DNA provides promising potential in forensic, clinical and pharmaceutical applications.[1] So far, various techniques have been developed for DNA detection, such as fluorescence, acoustic, atomic force microscopy, microfluidic system, surface plasmon resonance spectroscopy and quartz crystal microbalance,[2–4] ect. However, the disadvantages of time-consuming, poor precision and high cost expensiveness limit the practical application of these approaches. Alternatively, the electrochemical methods, mainly based on DNA electrochemical biosensors attract considerable interest in the past two decades owing to their simplicity, low-cost, portability, high selectivity and sensitivity as well as compatibility with microfabrication technology.[5] Although many new strategies such as nanoparticles labeling,[6] enzyme-assisted target recycling,[7] and molecule beacon[8] have been developed to improve the performance of DNA biosensors, the immobilization of DNA probes on the transducer surface is still a critical step in the biosensor construction process since it can effectively affect the sensitivity, accuracy and stability of the DNA biosensors.

During the last years, nano-sized materials received increasing attention in the construction of DNA biosensors, because they not only can greatly increase the loading amount of probe DNA, but also can act as a medium to amplify the electrochemical response in hybridization reaction. Therefore, various nanomaterials such as carbon nanotubes,[9] metal oxides[10] and nano-structured conducting polymers[11] have been utilized as probe DNA immobilization platforms. Since its discovery in 2004, a new kind of two-dimensional (2D) carbon material, graphene (GR) has also attracted much attention in fabricating biosensors due to its unique properties such as ballistic conductivity, high elasticity, mechanic strength, large surface-to-volume ratio and rapid heterogeneous electron transfer ability.[12–14] However, on the most common and economical method to prepare GR, i.e., through chemical reduction of graphene oxide (GONs), the hazardous chemical of hydrazine[15] or sodium borohydride[16] is needed as reductant, which not only increases the operating procedures of assays, but also possesses the potential risk of environmental pollutant. In addition, GR is hydrophobic and tends to form irreversible agglomerates or even restack to form graphite through strong π-π stacking or van der walls interaction under certain conditions.[17] Also, the lack of functional groups on the surface of GR make it difficult to immobilize the sensing molecules through covalent mode, which has been regarded as a most favorable mode in biosensor construction, because of its high stability and orientation.

[z]E-mail: fgao1981@126.com; axiang236@126.com

In contrast, the precursor for preparing the chemically reduced graphene, GONs show good hydrophilicity and dispersibility in water because it contains numerous hydrophilic functional groups, such as -OH, -COOH and epoxides on the basal plane and the sheet edge. Although the conductivity of GONs is not as high as graphene, it is still regarded as a good candidate for biosensing analysis because of its nano-effect, surface properties and good compatibility with biological molecules.[18] For example, based on its luminescence property and specific association with single-stranded DNA rather than double-stranded DNA, it has been exploited as a sensitive spectroscopic probe for DNA sensing analysis.[19,20] Additionally, it has also been applied as effective electrochemical nanocarriers to construct redox enzyme/protein biosensors[21,22] and immunosensor.[23] More recently, Bonanni et al.[24] constructed an electrochemical DNA biosensor for the detection of single nucleotides polymorphism relying on the inherent electrochemical response of GONs.

In this work, a novel DNA biosensor was fabricated, for the first time using GONs as a nano-scale and functional supporting platform for covalent immobilization of probe DNA (Figure 1). First, a layer of *L*-cystenine (*L*-cys) was assembled on gold electrode (AuE) through Au-S chemistry. Then the GONs were immobilized on the electrode surface through the reaction of activated carboxylic groups with the amino group of *L*-cys. Finally, the amino-modified probe DNA was anchored onto the electrode surface by coupling with the rest carboxylic groups of GONs. Due to the nanometer size and the multiple-site effects of GONs, the density of probe DNA of the fabricated biosensor was determined to be as high as 5.72×10^{-10} mol cm^{-2}. Hybridization experiments further showed that using a redox-active probe of methylene blue (MB) as the indicator, a wide kinetic range from 1.0×10^{-15} M to 1.0×10^{-9} M with a low detection limit of 5.0×10^{-16} for the target DNA can be quantified by the biosensor. Also the complementary, non-complementary and one-base-mismatched sequences can be well distinguished by the biosensor.

Experimental

Reagents.— Graphite and ethylenediaminetetraacetic acid (EDTA) were obtained from Guangdong Xilong Chemical Co. Ltd. (China); *L*-cystenine (*L*-cys) was purchased from Chinese Medicine Group Chemical Regent Co., Ltd (China); 1-(3-Dimethylaminopropyl)-3-ethylcarbodiimide hydrochloride (EDC) and N-Hydroxysuccinimide (NHS) were purchased from Shanghai Jingchun Reagent Co., Ltd (China); Tris (hydroxymethyl) aminomethane (Tris) was provided by Aladdin Reagent Company (China). Methylene blue (MB) and the other chemicals were of

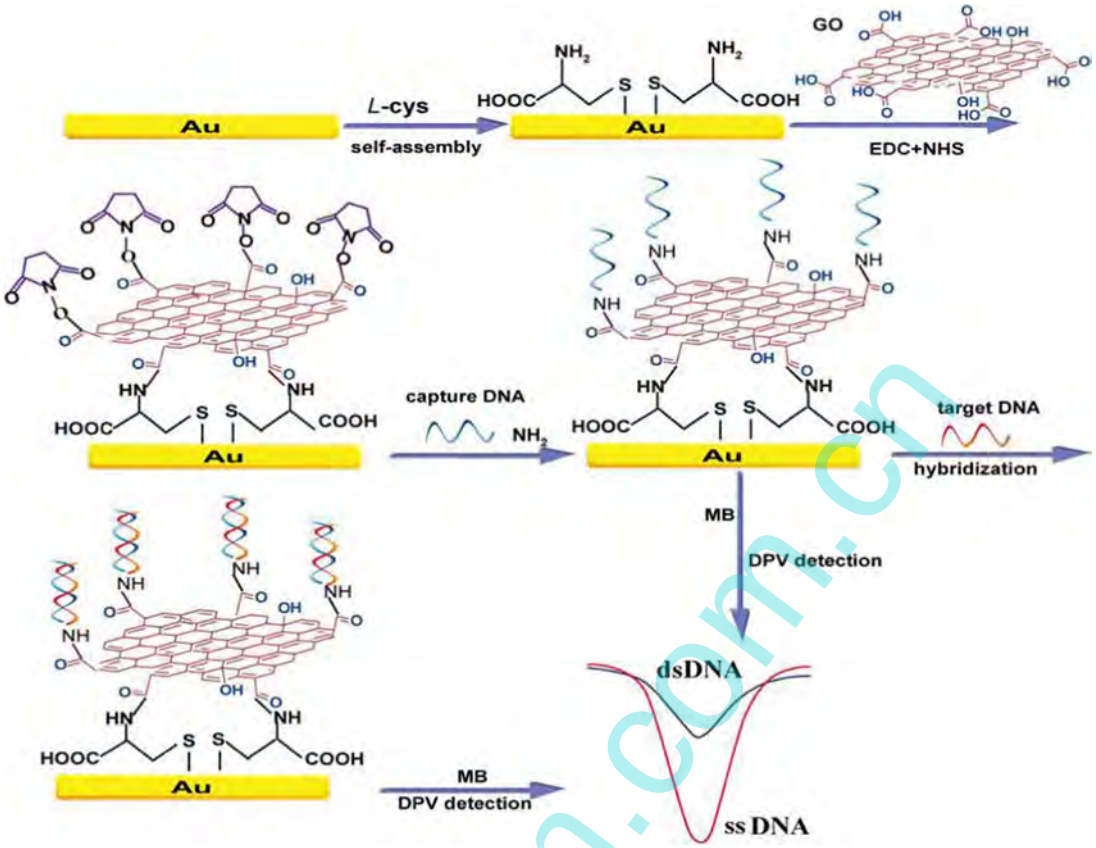

Figure 1. Schematic diagram for covalent immobilization of amino-modified probe DNA on GONs/*L*-cys/AuE and its hybridization application.

analytical reagent grade and were purchased commercially. Phosphate buffer solution with pH 6.86 was prepared by mixing 0.02 M NaCl and 0.5 M NaH_2PO_4-Na_2HPO_4. Doubly distilled water (DDW) was used throughout this experiment.

The 18-base synthetic oligonucleotides from cauliflower mosaic virus 35S (CaMV35S) promoter sequence were purchased from Shanghai Sangon Bio-engineering Co. Ltd. (China). Their base sequences were as follows:

- Capture probe sequence (S1): 5′- TCT TTG GGA CCA CTG TCG-3′
- Complementary sequence (S2): 5′-CGA CAG TGG TCC CAA AGA-3′
- One-base mismatched sequence (S3): 5′-CGA CAG TGG TCC CAA CGA-3′
- Three-base mismatched sequence (S4): 5′-CGA CAA TGG CCC CAA CGA-3′
- Non-complementary sequence (S5): 5′-GCA TCG AGC GAG CAG GTA-3′

Stock solutions of all above oligonucleotides were prepared with TE buffer solution (0.01 M Tris-HCl, 0.01 M EDTA, pH 8.0) and kept frozen.

Apparatus.— The morphology of the synthesized GO was examined by FEI Tecnai G20 transmission electron microscopy (TEM, USA). Fourier transform infrared (FT-IR) spectroscopy was recorded on an FT-IR spectrophotometer (Nicolet iS 10, USA). Electrochemical experiments including cyclic voltammetry (CV), electrochemical impedance spectroscopy (EIS) and differential pulse voltammetry (DPV) were measured on a CHI 650C electrochemical analyzer (Shanghai CH Instrument, China). A conventional three-electrode system was applied, which was consisted with a bare or modified AuE working electrode, a platinum wire auxiliary electrode and an Ag/AgCl reference electrode. The geometrical area of the working electrode was estimated to be 0.071 cm^2 according to diameter of the disk. AFM images were obtained with CSPM 5500 scanning probe microscope (China).

Preparation of graphite oxide.— The GO was prepared according to a modified Hummer's method using graphite power as starting material.[25] Briefly, 1 g natural-flake graphite and 0.5 g $NaNO_3$ were firstly reacted with 23 mL concentrated sulfuric acid in ice bath for 30 min. Then, 3 g $KMnO_4$ was slowly added and went on reacting for 2 h. Afterwards, the mixture was heated to 35°C and maintained for 30 min, followed by slow adding 46 mL water and going on reacting at 98°C for another 15 min to fully oxidize graphite. After cooling with water-bath, the reaction mixture was diluted with 140 mL water and 3 mL H_2O_2 (30%). After the mixture was purified by filter, multiple washing with 5% HCl and water, centrifugation and decanter, the precipitate was dialyzed for 7 days in DDW to remove the residual acid until the pH was close to 7. Finally, the product was dried by vacuum overnight at room temperature.

Fabrication of S1/GONs/L-cys/AuE and the hybridization reaction.— Prior to modification, the gold electrode was polished to a mirror-like surface with 1.0, 0.3 and 0.05 μm α-Al_2O_3, respectively, and rinsed ultrasonically with DDW, absolute ethanol and DDW, in turn. Then, the electrode was immersed in Piranha solution (V (H_2SO_4): V (H_2O_2) = 7:3) for 20 min. Furthermore, the gold electrode was electropolished via a cyclic voltammetry process, with the potential scanning from −0.2 to +1.6 V in 0.5 M H_2SO_4 at a scan rate 0.05 V s^{-1} for 50 cycles until steady curves were achieved and then dried with N_2 stream after washing with DDW.

After the surface pretreatment, the electrode was immersed in a PBS solution containing 1.0 × 10^{-5} M *L*-cys at 4°C for 24 h,

and then rinsed thoroughly with PBS and dried with N_2 stream. The modified electrode was recorded as *L*-cys/AuE. Followed by, 10 μL 1 mg mL^{-1} GONs that has been pre-mixed with 5.0×10^{-3} M EDC and 8.0×10^{-3} M NHS for 2 h was dropped on the surface of *L*-cys/AuE for dryness at room temperature, by which the GONs was anchored to *L*-cys/AuE and the obtained electrode was denoted as GONs/*L*-cys/AuE. Immobilization of probe DNA (S1) on GONs/*L*-cys/AuE was performed by immersing the GONs/*L*-cys/AuE electrode in 200 μL of 1.0×10^{-7} M S1 solution for 24 h. The electrode was then rinsed with TE buffer solution to remove the physically absorbed S1, thus a probe DNA modified electrode (S1/GONs/*L*-cys/AuE) was prepared. The hybridization reaction was performed by immersing S1/GONs/*L*-cys/AuE into 200 μL analytes solution (S2, S3, S4 or S5) with desired concentration for 40 min at 42°C, and then rinsed with TE buffer to remove the non-specifically adsorbed DNA.

Electrochemical measurements.— Electrochemical characterization on the biosensor fabrication process was carried out in 1.0×10^{-3} M $[Fe(CN)_6]^{3-/4-}$ solution containing 0.1 M KCl via cyclic voltammetry (CV) within the potential range from −0.2 V to +0.6 V, scan rate 0.1 V s^{-1}. The electrochemical impedance spectroscopy (EIS) was collected at a potential of +0.2 V in the frequency range from 0.01 Hz to 10^4 Hz with the voltage amplitude of 5 mV. The hybridization reaction was monitored by the following procedures: the S1/GONs/*L*-cys/AuE or its hybridized electrode was first immersed into 5.0×10^{-5} M MB solution for 15 min, and then transferred into the PBS supporting electrolyte solution to record with CV and differential pulse voltammetry (DPV). The CV was scanned between −0.6 V and 0 V. The DPV was recorded within the potential range from −0.6 V to 0 V under a pulse amplitude 0.05 V, pulse width 0.05 s, pulse period 0.2 s.

Results and Discussion

TEM and IR characterization of the synthesized GO.— Figure 2A shows the typical TEM image of the synthesized GO. From the result it could be clearly observed that the synthesized GO presented the crumpled and flake structure, which was very like the typical morphology of the GO reported in literature.[26] The successfull synthesis of the GO was further characterized by the FT-IR, and the result was displayed in Figure 2B. As seen, the sample had the characteristic peaks at 3416 cm^{-1} for the -OH stretching vibrations, 1735 cm^{-1} for C=O stretching of COOH groups, 1618 cm^{-1} for skeletal vibrations of un-oxidized graphitic domains, 1066 cm^{-1} for O-H deformations of the C-OH groups, and 1223 cm^{-1} for epoxy symmetrical ring deformation vibrations. These results further confirmed the successful synthesis of the GO in this work.

Atomic Force Microscopy (AFM) and electrochemical characterization of the biosensor.— Atomic force microscopy (AFM) has been used extensively to probe the nanoscopic structure of the modified surface due to its high accuracy.[27] The stepwise assembly of *L*-cys and GONs on the gold disk electrode (AuE) was first characterized by AFM. Figure 3 shows the typical topographic (a), cross-sectional (b) and three-dimensional (c) images of bare AuE (A), *L*-cys/AuE (B) and GONs/*L*-cys/AuE (C). As well seen, the cleaned bare AuE shows a flat and smooth characteristic (images a and c in Figure 3A) with the largest peak height of 66.51 nm (images b in Figure 3A). Upon self-assembly with *L*-cys, it was found that some raised regions appeared (images a and b in Figure 3B), and the largest peak height was significantly increased to 159.69 nm. These changes suggested that *L*-cys had been successfully assembled on the gold electrode. When the electrode of *L*-cys/AuE was further grafted with GONs, the independent peaks on *L*-cys/AuE were changed to some hill-like peaks (images a and c in Figure 3C), and the peak height was further increased to 205.01 nm, which clearly suggested that the nano-sized GONs have also been anchored on the electrode surface.

The stepwise modification process of different materials on the electrode surface was further characterized by CV (Figure 4A) and

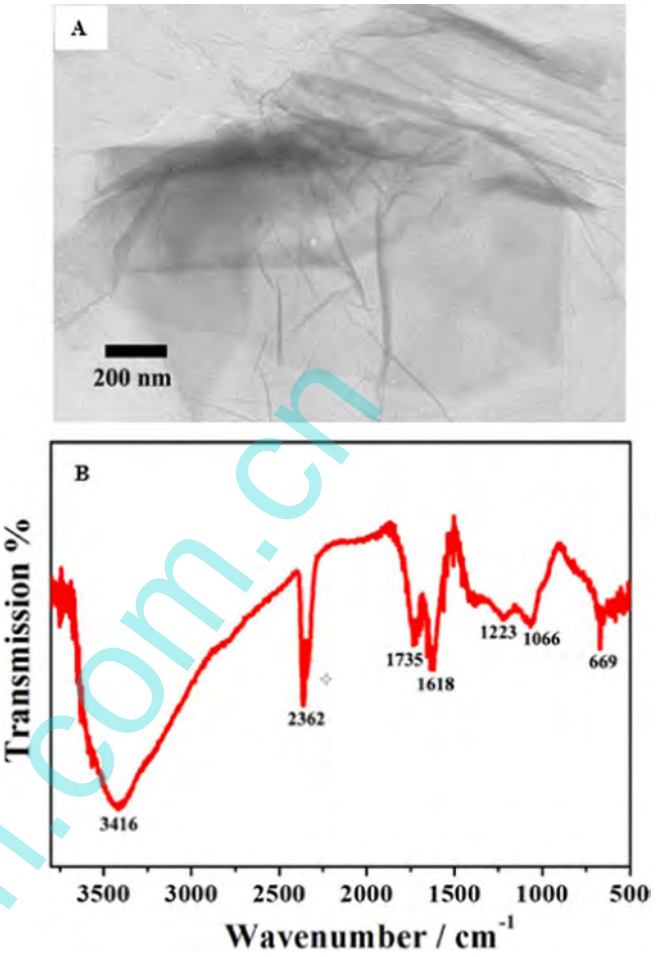

Figure 2. TEM images (A) and IR spectra (B) of GO.

EIS (Figure 4B). For a bare gold electrode, a couple of well-defined redox peaks of $[Fe(CN)_6]^{3-/4-}$ with the peak-to-peak separation (ΔE_p) of 73 mV were observed (Figure 4A, curve a). When the bare AuE was treated with *L*-cys, the redox peaks of $[Fe(CN)_6]^{3-/4-}$ showed decrease (Figure 4A, curve b), indicating that the *L*-cys molecules had been assembled on the gold electrode via the Au-S chemistry.[28–30] After the modified film of *L*-cys was further reacted with GONs, the redox peaks of $[Fe(CN)_6]^{3-/4-}$ decreased significantly and the ΔE_p was increased to 124 mV (Figure 4A, curve c). This indicated that GONs had also been successfully immobilized on the electrode surface, and blocked the electron transfer of $[Fe(CN)_6]^{3-/4-}$ ions to the electrode surface.[24]

EIS is a convenient and sensitive tool to probe the interface properties of the modified electrodes, which can give detailed information about the impedance changes in the modification process.[31,32] In this work, the fabrication of the biosensor was also monitored by EIS, and the obtained Nyquist plots were shown in Figure 4B. Inset showed the general electrical equivalent circuit for simulating the electrochemical processes. In this circuit, the parameter R_s represents the solution resistance and R_{ct} is the charge transfer resistance, which describes the counter-ions transfer occurring at the film/electrolyte interface. The diffusion of the counter ions through the film is described by Warburg element *W*, and the element Q_{dl} is the double layer capacitance. Among these elements, the R_{ct} is the most directive and sensitive parameter that responds to changes on the electrode interface.[33] The fitting results showed that the equivalent circuit model has a good agreement with the real experimental data. Table I summarized the parameters obtained by fitting analysis. From the result, The R_s component in terms of the solution resistance remained constant

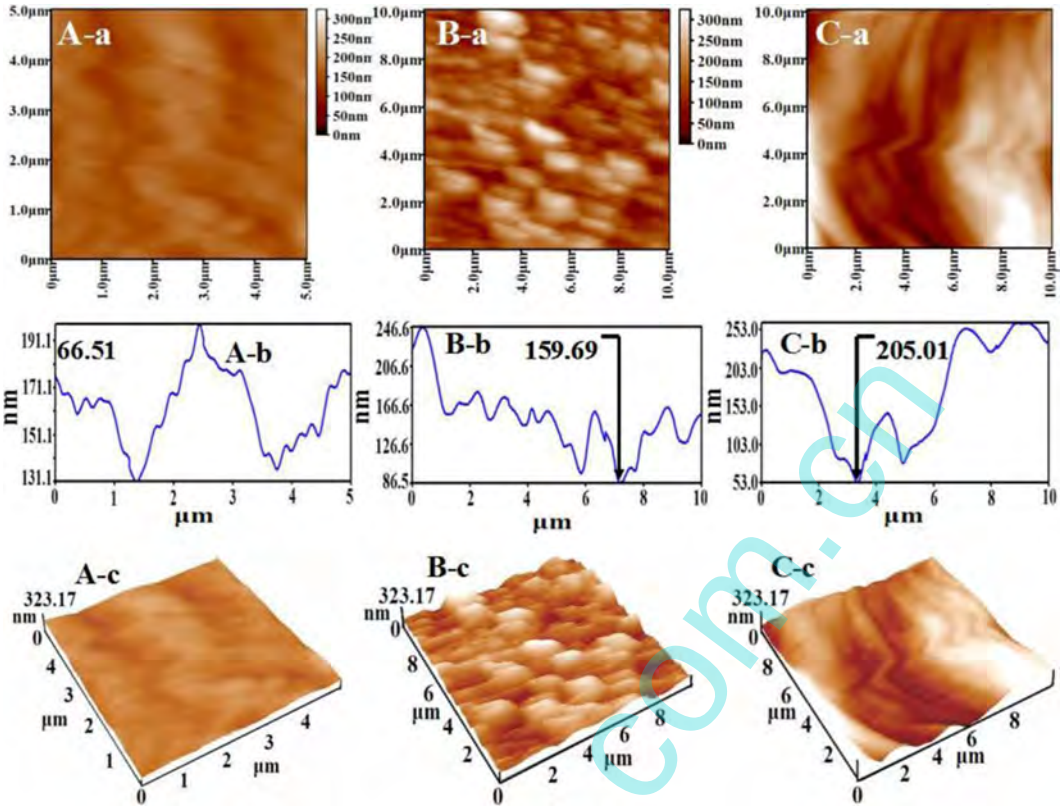

Figure 3. AFM images of (a) topographic (b) cross-sectional and (c) three- dimensional graph of bare AuE (A), *L*-cys/AuE (B) and GONs/*L*-cys/AuE (C).

at 6.76–7.83 Ω cm^2, as would be expected for measurements under identical conditions of supporting electrolyte concentration and temperature. In addition, from the fitting result it was found that a small R_{ct} value of 13.1 Ω cm^2 was observed on bare AuE (Figure 4B, curve a). When the AuE was modified with *L*-cys and GONs in turn, the values of R_{et} were increased to 48.1 Ω (Figure 4B, curve b) and 321.8 Ω (Figure 4B, curve c), respectively. These changes also confirmed that the *L*-cys and GONs had been assembled on the electrode surface, and the results were in good consistence with those in above CV experiments.

Immobilization of probe DNA (S1) on the electrode surface.— It has been reported that the phenothiazine dye of methylene blue (MB) can bind specifically to the unpaired guanine bases of the single-stranded DNA.[34] Based on this feature, the dye has been frequently used as an electrochemical probe to investigate the immobilization of DNA on a interface as well as its hybridization performance.[35] In this work, the immobilization of probe DNA on GONs/*L*-cys/AuE was further investigated using MB as the redox-active probe. Figure 5A shows the CVs of MB pre-accumulated on S1/GONs/*L*-cys/AuE (a), GONs/*L*-cys/AuE (b) and S1/*L*-cys/AuE (c). Obviously, compared with the CV of MB on GONs/*L*-cys/AuE, a pair of significantly increased redox peaks was observed on S1/GONs/*L*-cys/AuE, suggesting that the probe DNA had been successfully grafted to GONs and more MB molecules were adsorbed on the electrode surface through interaction with probe DNA strands. In addition, in order to probe the influence of GONs on immobilization amount of probe DNA, the electrochemistry of MB on S1 that directly grafted with *L*-cys/AuE was also investigated, and the CV was displayed as curve c in Figure 5A. Clearly, the redox peak intensity of MB on S1/*L*-cys/AuE was obviously weaker than that on S1/GONs/*L*-cys/AuE, suggesting that more MB molecules had been attached on the electrode surface of S1/GONs/L-cys/AuE.

In addition, according to the method provided by Zhang et al.,[36] the surface densities of probe DNA (Γ) anchored on the two electrode surfaces were calculated and compared. First, from the CV curve of MB on S1/GONs/*L*-cys/AuE, the charge quantity (*Q*) of MB was obtained to be 4.4 × 10^{-5} C, which corresponded to the molar quantity (*N*) of 2.3 × 10^{-11} mol as calculated according to the equation of $N = Q/neN_A$, where *n* (=2) is the number of electrons participating in the electrode reaction of MB; *e* (=1.6 × 10^{-19} C) the charge quantity of one electron; *N* (=6.02 × 10^{23} mol^{-1}) the Avogadro's number. In addition, since one MB molecule combined with one guanine base, and each probe strand contained five bases, so the immobilized amount of DNA on the electrode surface should be 4.05 × 10^{-11} mol via the stoichiometric ratio of 1:5. When the electrode surface area was further considered, the value of Γ, i.e., the surface density of probe DNA on was estimated to be 5.72 × 10^{-10} mol cm^{-2}. Similarly, the value of Γ on *L*-cys/AuE was determined to be 9.29 × 10^{-12} mol cm^{-2}, which was obviously lower than that on S1/GONs/*L*-cys/AuE. Therefore it could be more certain to identify that GONs played an important role to enhance the surface density of biomolecule on a biosensor due to its surface area effect and multi-site feature. Figure 5B shows the CVs of MB on S1/GONs/*L*-cys/AuE at the scan rate (υ) changed from 0.02 V s^{-1} to 0.35 V s^{-1}. It could be well seen that the redox peaks of MB varied with the change of the scan rate, and the oxidation peak currents (I_{pa}) and reduction peak current (I_{pc}) showed good linear relationships with υ with the regression equations of I_{pa} (μA) = −25.43 υ (V/s) −0.5138 (r = 0.9976) and I_{pc} (μA) = 25.07 υ (V/s) + 1.967 (r = 0.9929) (Inset of Figure 5B), respectively, which experimentally confirmed that MB had been adsorbed on the S1/GONs/*L*-cys/AuE.[37]

Analytical performance of the biosensor.— The analytical performance of the developed biosensor including selectivity and sensitivity was further evaluated using MB as the electroactive indicator. In order to obtain the most sensitive signals, the accumulation time of S1/GONs/*L*-cys/AuE in MB solution was first optimized. The results showed that when the incubation time of S1/GONs/*L*-cys/AuE in MB solution was increased, the electrochemical response of MB gradually

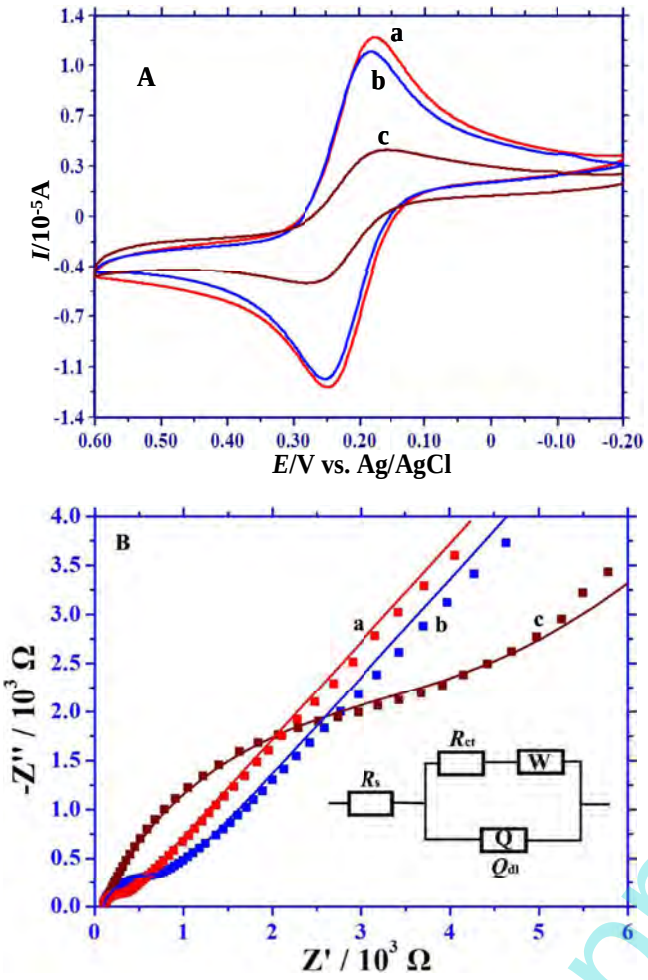

Figure 4. CVs (A) and EIS (B) image of 1.0×10^{-3} M $[Fe(CN)_6]^{3-/4-}$ with 0.1 M KCl at bare AuE (a), *L*-cys/AuE (b), GONs/*L*-cys/AuE (c)

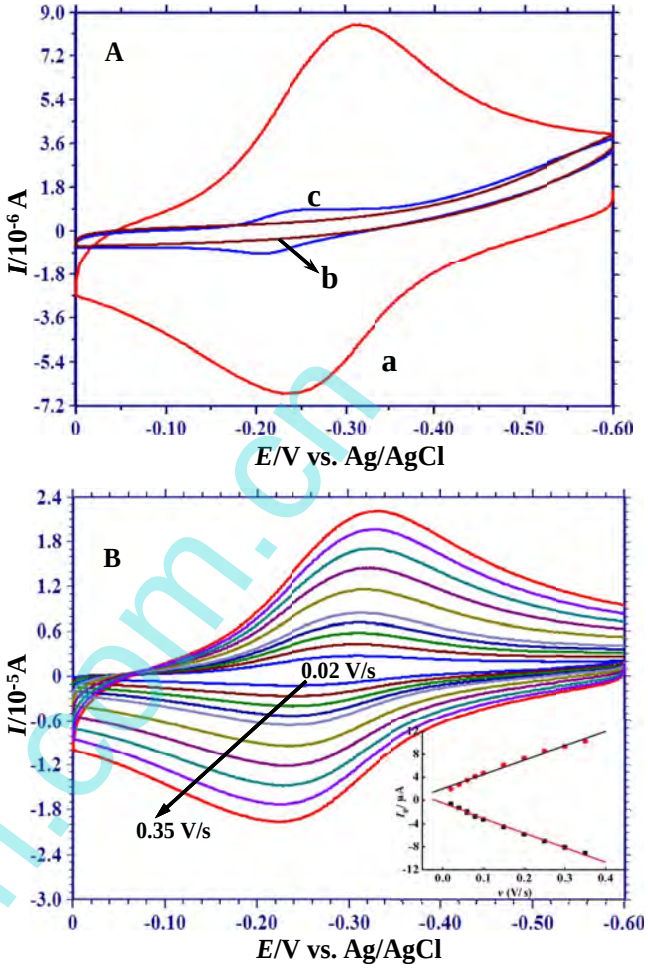

Figure 5. (A) CVs of 5.0×10^{-5} M MB at S1/GONs/*L*-cys/AuE (a), GONs/*L*-cys/AuE (b) and S1/*L*-cys/AuE (c) at the scan rate of 0.1 V s^{-1}. (B) CVs of 5.0×10^{-5} M MB absorbed on S1/GONs/*L*-cys/AuE at the different scan rates. Inset: Plot of peak current (I_p) versus scan rate (v).

increased. After an incubation time of 15 min, the electrochemical signal reached its maximum value and became constant, which suggested that the probe DNA on the biosensor had absorbed sufficient amount of MB molecules. Therefore, 15 min was chosen as the optimal binding time for MB.

The selectivity of the developed biosensor was investigated by hybridization with various DNA sequences. Figure 6 shows the DPVs and the corresponding bar chart (inset) for the oxidation peaks of MB at S1/GONs/*L*-cys/AuE before (curve a) and after hybridization with the complementary sequence of S2 (curve b), one-base mismatched sequence of S3 (curve c), three-base mismatched sequence of S4 (curve d), and non-complementary sequence of S5 (curve e). The largest signal was obtained at S1/GONs/*L*-cys/AuE, because MB has a strong affinity with the free guanine bases on unpaired probe DNA.[34] After the biosensor was hybridized with S2, significant decrease in the oxidation signal of MB was observed, which could be ascribed to the reason that the interaction between MB and guanine residues of S1 was prevented due to the formation of the perfect duplex structure between S1 and S2. The signal of MB at S5-S1/GONs/*L*-cys/AuE was very close to that at S1/GONs/*L*-cys/AuE, suggesting that the hybridization event between S5 and S1 had not happened. After hybridization with S3 and S4, and the results (curve c and curve d, respectively) showed that the DPV signals was diminished obviously in comparison with that on S1/GONs/*L*-cys/AuE, but was still higher than that on S2 hybridized electrode, suggesting that partial hybridization was happened between S1 and these two mismatched sequences. These results therefore indicated that, the developed biosensor had excellent hybridization selectivity for discriminating the complementary sequences from the base mismatched sequences and the non-complementary sequences.

The sensitivity of the DNA biosensor was evaluated by hybridization with the different concentrations of the complementary sequence of S2. Figure 7 shows the DPVs of MB on S1/GONs/*L*-cys/AuE after hybridization with increasing amount of S2. It was found that the peak currents in DPV response of MB decreased with the increase of the concentration of S2 (C_{S2}), which demonstrated that more and

Table I. Simulated result of the equivalent circuit elements for the different modified electrodes.

Electrode	R_s (Ω cm^2)	Q_{dl} (μF cm^2)	n	R_{ct} (Ω cm^2)	W (mΩ cm^2)
AuE	7.83	19.15	0.99	13.1	4.699
L-cys/AuE	6.76	162.0	0.78	48.1	4.531
GONs/*L*-cys/AuE	7.63	816.3	0.75	321.8	5.475

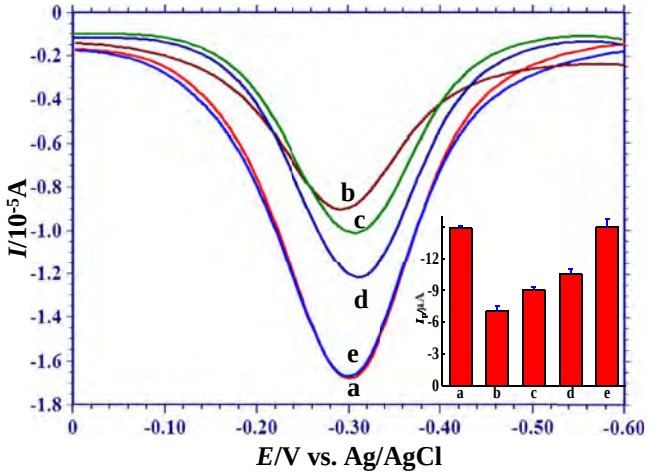

Figure 6. DPVs of 5.0×10^{-5} M MB at S1/GONs/*L*-cys/AuE before (a) and after hybridization with complementary sequence of S2 (b), one-base mismatched sequence of S3 (c), three-base mismatched sequence of S4 (d), and non-complementary sequence of S5 (e). All the concentrations of hybridized sequences were 1.0×10^{-13} M. Inset: Bar chart of the oxidation peak current (I_p) of MB on different hybridized electrodes.

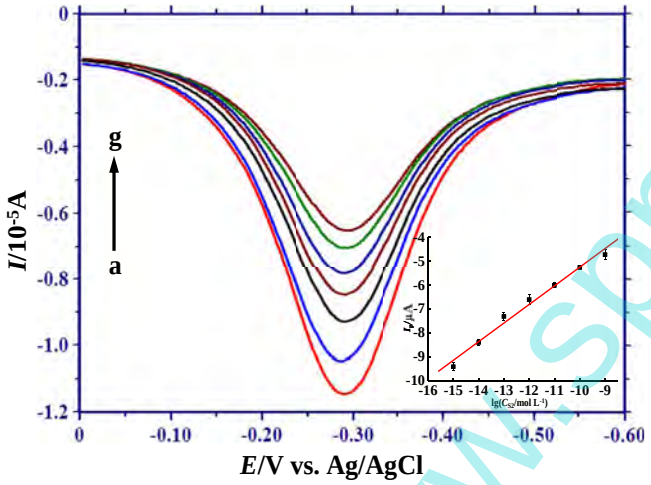

Figure 7. DPVs of 5.0×10^{-5} M MB on S1/GONs/*L*-cys/AuE hybridization with 1.0×10^{-15} M (a), 1.0×10^{-14} M (b), 1.0×10^{-13} M (c), 1.0×10^{-12} M (d), 1.0×10^{-11} M (e), 1.0×10^{-10} M (f), 1.0×10^{-9} M (g) S2. Inset: Relationship of I_p and the logarithm values of S2 concentration ($\lg C_{S2}$).

more double-helix DNA were formed on the electrode surface, and the bound MB amounts decreased accordingly. The values of peak currents of MB revealed an excellent correlation with logarithmic values of C_{S2} ($\lg C_{S2}$) ranging from 1.0×10^{-15} M to 1.0×10^{-9} M (inset in Figure 7) with a regression equation of $I_p/\mu A = 0.7750 \lg(C_{S2}/M) + 2.4824$, r = 0.9926. The detection limit was then estimated to be 5.0×10^{-16} M based on the signal-to-noise characteristic (S/N = 3). The analytical performance of this proposed biosensor was also compared with that of some other DNA electrochemical biosensors on the basis of GONs or graphene materials. The results are listed in Table II. Of the biosensors listed in the table, the present DNA biosensor exhibited the lowest detection limit for the target DNA. We think that the high sensitivity of the biosensor, on the one hand, is related to the high surface density of probe DNA, and on the other hand is related to the good water solubility of the GONs platform. Because the probe DNA is anchored on the water-soluble GONs, making the sensing interface had good hydrophilicity. Thus, the hybridization reaction of the probe DNA with the target strands was happened in a quasi-homogeneous liquid phase, which had been reported to handle fast hybridization speed and high hybridization efficiency. In addition, the probe DNA strands distributed on the surface of GONs had better flexibility and freedom than those directly immobilized at the conventional electrode surface, which is also benefit to improve the hybridization efficiency.

Reproducibility and stability of the DNA biosensor.— The reproductivity and stability are important properties of a DNA biosensor. In this work, the reproductivity of the biosensor was monitored by six parallel-made DNA biosensors to detect 1.0×10^{-13} M target DNA, and the results showed that a relative standard deviation (R.S.D) of 5.0% (n = 5) was estimated, showing a high reproducibility of the constructed DNA biosensor. Store of S1/GONs/*L*-cys/AuE at 4 °C for two weeks resulted in a change of 3.8% in the initial response, suggesting a good stability of the biosensor.

Conclusions

Graphene oxide nanosheets (GONs) have brought a lot of advantages upon electrochemical DNA detection. In this work, an ultrasensitive electrochemical DNA biosensor was fabricated using GONs as a multiple-site platform for probe DNA. When the biosensor was used to detect DNA, a wide dynamic range from 1.0×10^{-15} M to 1.0×10^{-9} M and a low detection limit of 5.0×10^{-16} M were obtained, which could be ascribed to the high loading density of probe DNA on the GONs with nano-size effect and multiple active sites characteristics. Selectivity assay showed that the biosensor had impressive selectivity with successful discrimination of the target DNA from other sequences including one-base mismatched, three-base mismatched, and non-complementary sequences. These results demonstrate the

Table II. Comparison of the analytical parameters of the proposed biosensor with the others.

DNA immobilization platform	Detection method (indicator)	Detection limit (M)	Linear ranges (M)	Refs
GONs/PLLY/GCE	DPV (MB)	1.69×10^{-13}	$1.0 \times 10^{-12} - 1.0 \times 10^{-6}$	14
GR-TiO_2-CTS/CILE	DPV (MB)	7.21×10^{-13}	$1.0 \times 10^{-12} - 1.0 \times 10^{-6}$	35
Au/GR/CILE	DPV (MB)	2.9×10^{-13}	$1.0 \times 10^{-12} - 1.0 \times 10^{-6}$	38
AuNPs/rGO/GCE	DPV (adriamycin)	3.5×10^{-14}	$1.0 \times 10^{-13} - 1.0 \times 10^{-8}$	39
p-RGO/CILE	DPV (MB)	2.9×10^{-13}	$1.0 \times 10^{-12} - 1.0 \times 10^{-6}$	40
Au/GO/GCE	DPV (MB)	-	$1.0 \times 10^{-13} - 1.0 \times 10^{-9}$	41
GA/Th-G/GA/Cys/AuE	DPV (daunomycin)	1.26×10^{-13}	$1.0 \times 10^{-12} - 1.0 \times 10^{-7}$	42
PXa-ERGNO/GCE	EIS ($[Fe(CN)_6]^{3-/4-}$)	4.2×10^{-15}	$1.0 \times 10^{-14} - 1.0 \times 10^{-8}$	43
Au-PDI-graphene/GCE	EIS ($[Fe(CN)_6]^{3-/4-}$)	1.2×10^{-15}	$1.0 \times 10^{-14} - 1.0 \times 10^{-10}$	44
GONs/*L*-cys/AuE	DPV (MB)	5.0×10^{-16}	$1.0 \times 10^{-15} - 1.0 \times 10^{-9}$	This work

Note: CTS: chitosan; AuNPs: Au nanoparticles; PLLY: poly-L-lysine; CILE: carbon ionic liquid electrode; GCE: glassy carbon electrode; rGO: reduced graphene oxide; p-RGO: partially reduced graphene oxide; GA: glutaraldehyde; Th-G: thionine-graphene; PXa-ERGNO: poly(xanthurenic acid, Xa)-reduced graphene oxide; PDI : perylenetetracarboxylic acid di-imide

potential of the developed biosensor to meet the inexpensive, rapid, and handy detection of DNA in real samples.

Acknowledgments

The work is supported by the National Natural Science Foundation of China (No. 21275127), Program for New Century Excellent Talents in Fujian Province University (No. JA12204) and Key Provincial University Project of Fujian (No. JK2011032).

References

1. A. A. Jamali, M. Pourhassan-Moghaddam, J. E. N. Dolatabadi, and Y. Omidi, *TrAC Trends Anal Chem*, **55**, 24 (2014).
2. O. Doluca, T. K. Hale, P. J. B. Edwards, C. González, and V. V. Filichev, *ChemPlusChem*, **79**, 58 (2014).
3. M. Bao and X. M. Ma, *Mater Sci Eng C*, **32**, 1808 (2012).
4. D. Pastré, V. Joshi, P. A. Curmi, and L. Hamon, *Small*, **9**, 3630 (2013).
5. D. L. Zheng, Q. X. Wang, F. Gao, Q. H. Wang, W. W. Qiu, and F. Gao, *Biosens Bioelectron*, **60**, 167 (2014).
6. H. Wang, R. Yang, L. Yang, and W. Tan, *ACS Nano*, **3**, 2451 (2009).
7. Q. Wang, C. Yang, Y. Xiang, R. Yuan, and Y. Chai, *Biosens Bioelectron*, **55**, 266 (2014).
8. X. Mao, H. Xu, Q. Zeng, L. Zeng, and G. Liu, *Chem Commun*, 3065 (2009).
9. M. Ligaj, M. Tichoniuk, D. Gwiazdowska, and M. Filipiak, *Electrochim Acta*, **128**, 67 (2014).
10. M. Tak, V. Gupta, and M. Tomar, *Biosens Bioelectron*, **59**, 200 (2014).
11. Z. H. Zhang, P. Liang, X. J. Zheng, D. L. Peng, F. F. Yan, R. Zhao, and C. L. Feng, *Biomacromolecules*, **9**, 1613 (2008).
12. X. Zhang, F. Gao, X. L. Cai, M. X. Zheng, F. Gao, S. L. Jiang, and Q. X. Wang, *Mater Sci Eng C*, **33**, 3851 (2013).
13. W. Guo, X. Cao, Y. Liu, X. Tong, and X. Qu, *J Electrochem Soc*, **161**(12), B248 (2014).
14. C. Gao, L. Hang, X.L. Liao, F. Gao, and Q.X. Wang, *Chin J Anal Chem*, **42**, 853 (2014).
15. S. Stankovich, D. A. Dikin, R. D. Piner, K. A. Kohlhaas, A. Kleinhammes, Y. Y. Jia, Y. Wu, S. B. T. Nguyen, and R. S. Ruoff, *Carbon*, **45**, 1558 (2007).
16. H. J. Shin, K. K. Kim, A. Benayad, S. M. Yoon, H. K. Park, I. S. Jung, M. H. Jin, H. K. Jeong, J. M. Kim, J. Y. Choi, and Y. H. Lee, *Adv Funct Mater*, **19**, 1987 (2009).
17. Y. Si and E. T. Samulski, *Nano Lett*, **8**, 1679 (2008).
18. D. Li, M. B. Muller, S. Gilje, R. B. Kaner, and G. G. Wallace, *Nat Nanotechnol*, **3**, 101 (2008).
19. S. J. He, B. Song, D. Li, C. F. Zhu, W. P. Qi, Y. Q. Wen, L. H. Wang, S. P. Song, H. P. Fang, and C. H. Fan, *Adv Funct Mater*, **20**, 453 (2010).
20. L. Gao, C. Q. Lian, Y. Zhou, L. R. Yan, Q. Li, C. X. Zhang, L. Chen, and K. P. Chen, *Biosens Bioelectron*, **60**, 22 (2014).
21. L. L. Zhang, H. H. Cheng, H. M. Zhang, and L. T. Qu, *Electrochim Acta*, **65**, 122 (2012).
22. W. Sun, S. X. Gong, F. Shi, L. L. Cao, L. Y. Ling, W. Z. Zheng, and W. C. Wang, *Mater Sci Eng C*, **40**, 235 (2014).
23. D. Du, L. M. Wang, Y. Y. Shao, J. Wang, M. H. Engelhard, and Y. H. Lin, *Anal Chem*, **83**, 746 (2011).
24. A. Bonanni, C.K. Chua, G. Zhao, Z. Sofer, and M. Pumera, *ACS Nano*, **6**, 8546 (2012).
25. W. S. Hummers and R. E. Offeman, *J Am Chem Soc*, **80**, 1339 (1958).
26. S. Dong, X. Dou, D. Mohan, C. Pittman Jr., and J. Luo, *Chem. Eng. J*, **270**, 205 (2015).
27. S. G. Ge, M. Yan, J. J. Lu, M. Zhang, F. Yu, J. H. Yu, X. R. Song, and S. L. Yu, *Biosens Bioelectron*, **31**, 49 (2012).
28. M. Y. Li, S. S. Huang, P. S. Zhu, L. M. Kong, B. Peng, and H. Gao, *Electrochim Acta*, **54**, 2284 (2009).
29. Y. Xue, H. Zhao, Z. J. Wu, X. J. Li, Y. J. He, and Z. B. Yuan, *Analyst*, **136**, 3725 (2011).
30. Q. Chen, J. Zhou, Q. Han, Y. H. Wang, and Y. Z. Fu, *Colloids Surf B*, **92**, 130 (2012).
31. B. B. Berkes, M. H. Huang, J. B. Henry, M. Kokoschka, and A. S. Bandarenka, *ChemPlusChem*, **79**, 348 (2014).
32. C. Y. Hu, D. P. Yang, Z. Y. Wang, L. L. Yu, J. L. Zhang, and N. Q. Jia, *Anal Chem*, **85**, 5200 (2013).
33. H. L. Guo, X. F. Wang, Q. Y. Qian, F. B. Wang, and X. H. Xia, *ACS Nano*, **3**, 2653 (2009).
34. P. Kara, K. Kerman, D. Ozkan, B. Meric, A. Erdem, P. E. Nielsen, and M. Ozsoz, *Electroanalysis*, **14**, 1685 (2002).
35. H. W. Gao, M. Sun, C. Lin, and S. B. Wang, *Electroanalysis*, **24**, 2283 (2012).
36. W. Zhang, T. Yang, C. Jiang, and K. Jiao, *Appl. Surf. Sci.* **254**, 4750 (2008).
37. Y. Jin, X. Yao, Q. Liu, and J. H. Li, *Biosens Bioelectron*, **22**, 1126 (2007).
38. W. Sun, X. W. Qi, Y. Y. Zhang, H. R. Yang, H. W. Gao, Y. Chen, and Z. F. Sun, *Electrochim Acta*, **85**, 145 (2012).
39. Y. Z. Zhang and W. Jiang, *Electrochim Acta*, **71**, 239 (2012).
40. W. Sun, Y. Y. Zhang, A. H. Hu, Y. X. Lu, F. Shi, B. X. Lei, and Z. F. Sun, *Electroanalysis*, **25**, 1417 (2013).
41. Z. J. Wang, J. Zhang, Z. Y. Yin, S. X. Wu, D. Mandler, and H. Zhang, *Nanoscale*, **4**, 2728 (2012).
42. L. M. Zhu, L. Q. Luo, and Z. X. Wang, *Biosens Bioelectron*, **35**, 507 (2012).
43. T. Yang, Q. H. Li, L. Meng, X. H. Wang, W. W. Chen, and K. Jiao, *ACS Appl Mater Interfaces*, **5**, 3495 (2013).
44. W. Zhang, F. H. Li, Y. W. Hu, S. Y. Gan, D. X. Han, Q. X. Zhang, and L. Niu, *J Mater Chem B*, **2**, 3142 (2014).